



Contents lists available at ScienceDirect

Tetrahedron

journal homepage: www.elsevier.com/locate/tet

Insight into hydrogen bonding of terephthalamides with amino acids: Synthesis, structural and spectroscopic investigations

Barbara Hachuła^{a,*}, Anna Polasz^a, Maria Książek^b, Joachim Kusz^b, Violetta Kozik^a, Marek Matussek^a, Wojciech Pisarski^a

^a Institute of Chemistry, University of Silesia, Szkolna 9, 40-006 Katowice, Poland

^b Institute of Physics, University of Silesia, Uniwersytecka 4, 40-007 Katowice, Poland

ARTICLE INFO

Article history:

Received 25 January 2017

Received in revised form

11 March 2017

Accepted 27 March 2017

Available online xxx

Keywords:

Hydrogen bond
Polarized IR spectra
Exciton coupling
H/D exchange
Terephthalamide

ABSTRACT

Several *bis*-terephthalamides based on methyl esters of amino acids including glycine (**1**), β -alanine (**2**), γ -aminobutyric acid (**3**) and ϵ -aminocaproic acid (**4**), $X-(CH_2)_n-HNOC-C_6H_4-CONH-(CH_2)_n-X$ ($X=CO_2CH_3$, $n=1, 2, 3$ and 5), have been synthesized and characterized by single-crystal X-ray diffraction and spectroscopic methods: FT-IR, polarized FT-IR, Raman, 1H NMR and ^{13}C NMR. The four structures assemble *via* classical $N-H\cdots O$ hydrogen bonds between amide functionalities linking the molecules into chains parallel to the short axis. The analysis of polarized IR spectra of pure and deuterated compounds reveals that a weak interchain (“*through-space*”) exciton coupling involves two closely-spaced hydrogen bonds belonging to two different adjacent chains. The exciton coupling magnitude decreases with the addition of methylene groups to the terephthalamide system. Isotope effects in terephthalamides show that the distribution of protons and deuterons in the crystalline lattice depends on the strength of the exciton couplings involving hydrogen bonds.

© 2017 Elsevier Ltd. All rights reserved.

1. Introduction

The great interest in the study of aromatic ester amides derived from natural amino acids is explained by the possibility of using them in the synthesis of potential families of biodegradable synthetic polymers for such applications as sutures, surgical implants, controlled-release formulations for drugs and scaffolds for tissue engineering.^{1–5} The poly(ester amide)s have ester and amide groups on their chemical structure which are of a degradable character and provide good thermal and mechanical properties. Particularly, poly(ester amide)s containing α -amino acids have risen as important materials in the biomedical field. The presence of the α -amino acid contributes to better cell–polymer interactions, allows the introduction of pendant reactive groups and enhances the overall biodegradability of the polymers.³ Thus we decided it would be interesting to construct model compounds derived from terephthalic acid, α -amino acids and different diols to study new polymer structures. Several terephthalamides have been reported so far.^{6–8} The crystal structures of a series of terephthalic

acid diamide derivatives in which the nitrogen atoms are mono- or disubstituted were described.⁶ All previously reported *bis*-terephthalamide structures self-assembled to form hydrogen-bonded supramolecular β -sheets, ribbon or helix.^{6–8}

Hydrogen bonding is responsible for the molecular and macroscopic properties of materials, molecular recognition and supramolecular structure.⁹ This kind of molecular interaction is ubiquitous in biological systems providing stability to the protein molecule and also stabilizing the structure of DNA by forming a bridge between the pyrimidine and purine bases. Due to many applications of hydrogen bonds related to understanding the dynamics of the processes in the hydrogen-bonded systems, it is important to find out how individual hydrogen bonds would respond to variations in temperature and to isotope dilution. The most popular methods to analyze changes in the intermolecular interactions are vibrational spectroscopy and X-ray diffraction.

Polarized IR spectroscopy is considered among the most efficient tools for hydrogen bond research, providing complete information about the coupling mechanisms involving these interactions in crystal lattices. In 1998, Flakus and Bańczyk¹⁰ studying polarized IR spectra of cyclic dimers noticed anomalous isotopic dilution effects. The authors have supposed the existence

* Corresponding author.

E-mail address: barbara.hachula@us.edu.pl (B. Hachuła).

of a new H/D isotopic recognition (*viz.* the H/D “self-organization”), depending on a non-random distribution of protons and deuterons in the lattices of isotopically diluted crystals. The origin of this anomalous arrangement of protons and deuterons between the hydrogen bonds was assigned to the new kind of co-operative interactions involving hydrogen bonds (*i.e.*, the dynamical co-operative interactions).¹¹ Similar experimental observations have been done in our several dozen works for systems with different kind of hydrogen bonded associates in the crystalline lattice, *i.e.*, chain, dimer, trimer, tetramer or hexamer.^{12a–12n} In a study made by Flakus et al.^{12a–12f} and Hachuta et al.^{12g–12n} a direct relationship between the temperature dependence of IR spectral properties and the electronic structure for H-bonded crystalline systems have been recently proved. For systems with aromatic hydrogen bonds (favourable electronic structure), governed by an intrachain (“tail-to-head” (TH)) exciton coupling mechanism, the lower-frequency branch of the $\nu_{\text{X-H}}$ band, recorded in the wide temperature range, was more intense in relation to the intensity of the higher-frequency band branch.^{12g,12k} In the case of systems with non-aromatic hydrogen bonds (unfavourable electronic structure), quite different spectral behavior can be observed, *i.e.*, the higher-frequency branch of the band was the most intense fragment of the spectrum at 293 K and 77 K. In these systems only interchain (“through-space” (TS)) exciton coupling mechanism involving pairs of closely-spaced hydrogen bonds is active. This coupling of the “side-to-side”-type occurred basically *via* the van-der-Waals forces.^{12l–12n}

Due to the importance of terephthalamides in biomaterials and tissue engineering, and also our hydrogen bond studies discussed above, it was considered worthwhile to determine crystal structures and to make polarized IR measurements on hydrogen- and deuterium-bonded terephthalamides. In addition to this, temperature dependent and isotopic infrared measurements on terephthalamide derivatives were also performed to investigate the influence of temperature and deuteration on the vibrational behavior of terephthalamides and draw some meaningful conclusions from the observed spectral changes. Thus, a considerable part of the presented work is devoted to analyze crystal structures of **1–4** in order to correlate the structures to the vibrational results. In the next part we extend the approach of our previous vibrational studies to terephthalamide systems to elucidate the nature of the co-operative interaction mechanisms involving hydrogen bonds in systems like infinite chains *via* a quantitative interpretation of the crystalline system spectra. Measurement of the IR spectra of terephthalamide derivatives were mainly focused on spectroscopic effects corresponding to the intensity distribution, the influence of temperature, the linear dichroism, and the isotopic substitution of deuterium recorded in the frequency range of the proton and the deuterium stretching vibration bands, *viz.* $\nu_{\text{N-H}}$ and $\nu_{\text{N-D}}$, respectively.

2. Results and discussion

2.1. Molecular geometry of compounds **1–4**

The crystal structure of **1** was re-determined in this study and is similar to that reported by Armelin et al.⁸ Compounds **2–4** have not been described earlier in the literature. The atomic numbering scheme for all four compounds is given in Figs. 1–4, which also show the contents of the asymmetric unit in each case and the crystal packing of the molecules. The selected crystallographic data and the melting points determined by differential scanning calorimetry (DSC) are summarized in Table 1. A full summary of the refinement details is given in Table S1 in the Supporting Information. The selected geometrical parameters are reported in

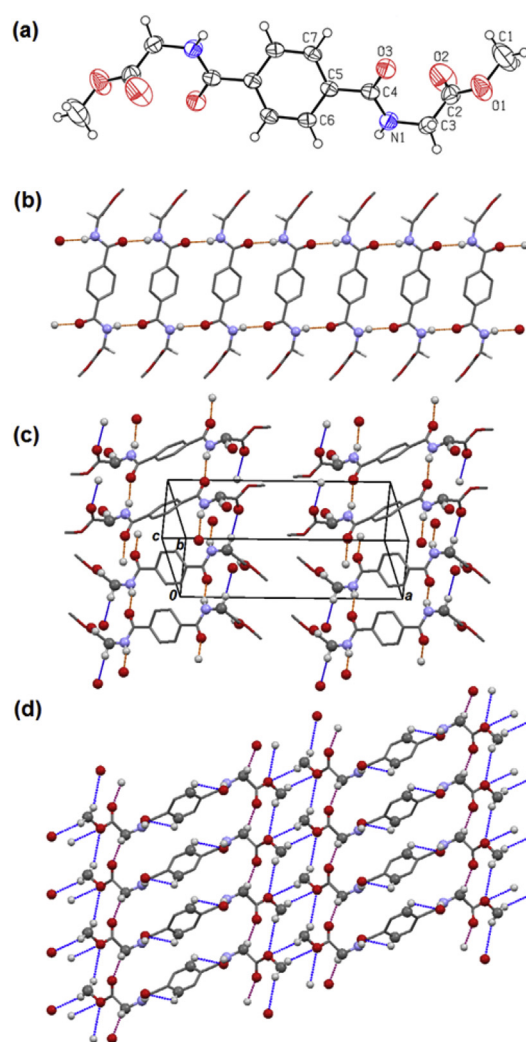


Fig. 1. (a) Molecular structure of **1** with atom labelling of the asymmetric unit; (b) the infinite 1D hydrogen bonding chain *via* N–H...O along the crystallographic *b* axis; (c) a part of 2D crystal structure showing the C(4) chains (d) 3D hydrogen-bonded network of **1** (*ac* plane).

Table S2. The strongest hydrogen-bonding interactions are shown in Table 2. The detailed values characterizing all interactions are collected in Table S3.

All the compounds crystallize with crystallographic inversion symmetry, with each asymmetric unit consisting of half a molecule (Figs. 1–4). The amide and ester groups and the benzene ring of **1–4** are essentially planar (r.m.s. deviations of 0.0056, 0.0219 and 0.0012 Å of **1**, 0.0019, 0.0266 and 0.0003 Å of **2**, 0.0141, 0.0104 and 0.0008 Å of **3**, 0.0278, 0.0276 and 0.0011 Å of **4** for $C_{\text{ipso}}-C_{\text{amide}}(=O)-N-C_{\text{amino}}$ acid, $C1-O1-C2(=O)-C3$ and $C_{\text{arom}}-C_{\text{arom}}$). The amide groups are rotated slightly out of the aromatic plane *i.e.* the interplanar angles between the benzene ring and the plane defined by $C_{\text{ipso}}-C(=O)-N-C$ atoms range from 25.82° to 28.02° (27.17° **1**, 28.02° **2**, 25.82° **3**, 26.89° **4**). The molecular conformation of **1–4** can be also determined by the $C_{\text{arom}}-C_{\text{ipso}}-C(=O)$ and the $C_{\text{arom}}-C_{\text{ipso}}-C_{\text{amide}}-N$ torsion angles which clearly deviated from 180° (–150.16(15)° and 155.30(14)° for **1**; 150.1(2)° and 153.7(2)° for **2**; 153.81(15)° and 155.38(14)° for **3**; –150.98(16)° and –153.47(15)° for **4**) (Table S2). The distances and angles within the four compounds reported are generally as expected, although the $C_{\text{amide}}=O$ bond length increases and the $C_{\text{amide}}-N$ bond length decreases with the increasing number of carbons in the amino acid

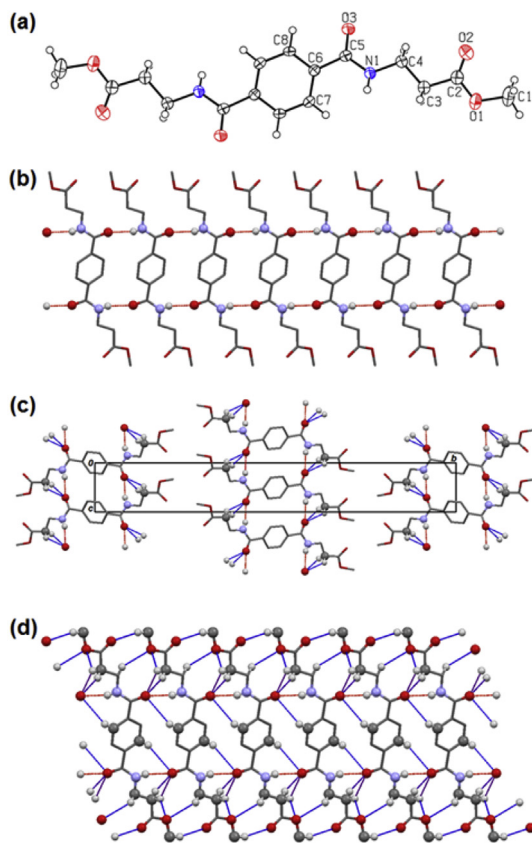


Fig. 2. (a) Molecular structure of **2** with atom labelling of the asymmetric unit; (b) the infinite 1D hydrogen bonding chain via N–H···O along the crystallographic *c* axis; (c) the molecular packing viewed along the *a* axis, showing the $R_2^1(6)$ rings, linked by C–H···O interactions; (d) 3D supramolecular framework of **2**.

side chains of **1–3**. Moreover, the $C_{amide}=O$ and the $C_{amide}-N$ distances in **4** are between these for **1** and **2**. The increase in side-chain length slightly alters the planar geometry of **1–4**, i.e., the ester groups are strongly twisted in **1** and **4** or lie in the plane of the amide group in **2** and **3** (see torsion angles in Table S2). The dihedral angle between these planes are $78.832(75)^\circ$ for **1**, $28.809(130)^\circ$ for **2**, $20.099(34)^\circ$ for **3** and 43.68° for **4**.

Compounds **1–4** are a disubstituted terephthalamides owning one NH function at each nitrogen atom. All the compounds self-assemble in a similar manner in which the molecules are connected by intermolecular N–H···O hydrogen bonds along the shorter crystallographic axis to form ribbon-like structures (Figs. 1–4). The crystal packing of compounds **1**, **2** and **4** is similar to each other, i.e., the molecules are stacked atop one another to form the unusual ladder motif involving rings of graph $setR_2^2(18)$.¹³ Neighbouring molecules of **1**, **2** and **4** in the ladder are related by translation and the repeat distance of the chain about 5 Å corresponds to the short *b*, *c* and *a* axis, respectively. On the other hand, each molecule of **3** is connected with four different adjacent molecules, two lower and two higher, leading to a crosslinked three-dimensional pattern (Fig. 3c). The strongest hydrogen bonds occur between the molecules of **3**, whereas the weakest H-bond interactions are found in **4**. The ester groups of **4** are considerably interlinked, while in terephthalamides **1** and **2** the methyl groups of –COOCH₃ system are adjacent to each other. Beyond classical N–H···O hydrogen bonds in **1**, **2** and **4**, there are also observed C–H···O interactions, mostly from the amino acid hydrogens. The “shorter” weak hydrogen bonds with C···O distances of up to 3.5 Å are described below and shown in Figs. 1c and 4c. The “longer”

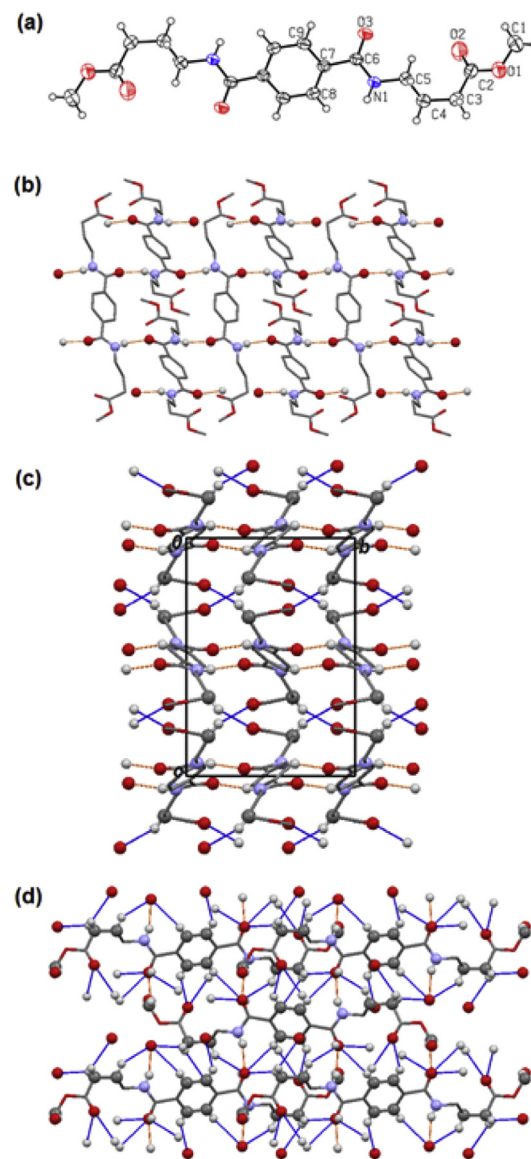


Fig. 3. (a) Molecular structure of **3** with atom labelling of the asymmetric unit; (b) the infinite 1D hydrogen bonding chain via N–H···O along the crystallographic *b* axis; (c) 2D molecular framework along the crystallographic *bc* plane; (d) 3D hydrogen-bonding architecture of **3**.

C–H···O hydrogen bonds ($C\cdots O > 3.5$ Å) are listed in Table S3 and also presented in Figs. 1–4.

The adjacent 1D chains of **1** are interconnected via hydrogen bonds C3–H3A···O2 to form a two-dimensional (2D) layer parallel to the *ac* plane (Fig. 1c). The neighboring molecules also join together via bifurcated hydrogen bonds, N1–H1···O3 and C6–H6···O3. In compound **4**, the terephthalamide molecules are bonded by a bifurcated (N1–H1···O3 and C6–H6B···O3) and a weak C3–H3A···O2 hydrogen bond to form layers parallel to the *ab* plane. The 2D sheets in **4** are fused together to yield a 3D network through the weak C–H···O hydrogen bonds (Fig. 4d). Interestingly, the structure of **2** exhibits a trifurcated C–H···O interaction motif with the amide oxygen atom acting as a hydrogen bond acceptor from two different C–H donors. These interactions involve two methylene C–H (C3–H3A···O3 3.249(3) Å; C3–H3B···O3 3.520(4) Å) and an amide N–H (N1–H1···O3 2.955(3) Å) acting as hydrogen bond donors, from a symmetry generated molecule

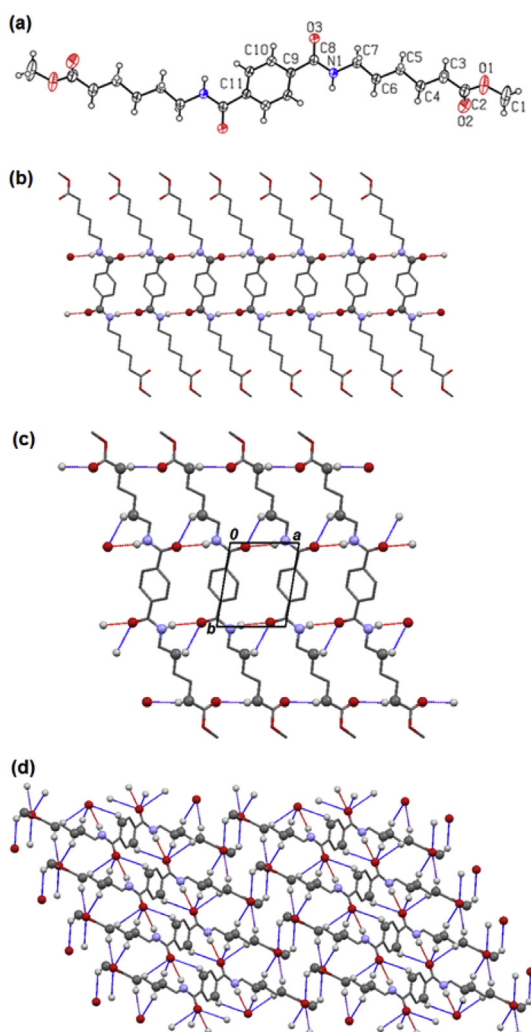


Fig. 4. (a) Molecular structure of **4** with atom labelling of the asymmetric unit; (b) the infinite 1D hydrogen bonding chains via N–H···O along the crystallographic *a* axis; (c) the molecular packing viewed along the *c* axis, showing the $R_2^1(6)$ rings, linked by C–H···O interactions (d) a view of the 3D hydrogen-bonded layer of **4**.

(*x*, *y*, $-1 + z$; $-1 + x$, *y*, $-1 + z$; *x*, *y*, $-1 + z$) (Fig. 2c). Compound **3** also exhibits one “shorter” weak hydrogen bond, namely C3–H3B···O2 (3.448(2) Å; $1 - x, -1/2 + y, 1/2 - z$), which connects the terminal regions of the butyl acetate chains of neighbouring molecules approximately the *b* axis to form layers parallel to the *ab* plane. In total the packing of compounds involves 5 (**1**) and 6 (**2–4**) weak hydrogen bonds and then the overall structures of **1–4** are a complex three-dimensional network (Figs. 1d–4d).

The adjacent benzene rings of the 2D layers of **1**, **2** and **4** are parallel displaced. The distances between the centers of the two aromatic rings within one stack are 4.969 Å for **1**, 6.202 Å for **2**, 10.004 Å for **3** and 5.209 Å for **4**. It is outside of the range of π – π stacking interactions (3.3–3.8 Å), and we conclude that π – π stacking interactions do not exist. The benzene rings from two different stacks of **1** make a dihedral angle of 73.07° with a distance of 5.13 Å between the central point of them. The angles between the aromatic rings of molecules belonging to two different stacks in compounds **2** and **3** are 47.72° and 24.46°, respectively.

2.2. Hirshfeld surface analysis of **1–4**

The Hirshfeld surfaces mapped with d_{norm} for the molecules of

Table 1
Crystallographic data and the melting points of the compounds **1–4**.

	1	2	3	4
CCDC numbers	1005546	1005547	1005548	1511353
Melting point [° C] ^a	163	214	177	157
Formula	C ₁₄ H ₁₆ N ₂ O ₆	C ₁₆ H ₂₀ N ₂ O ₆	C ₁₈ H ₂₄ N ₂ O ₆	C ₂₂ H ₃₂ N ₂ O ₆
Compound weight	308.29	336.34	364.39	420.49
Crystal system	Monoclinic	Monoclinic	Orthorhombic	Triclinic
Space group	<i>P2</i> ₁ / <i>c</i>	<i>P2</i> ₁ / <i>n</i>	<i>Pbca</i>	<i>P</i> $\bar{1}$
Temperature, K	298 (2)	298 (2)	298 (2)	294 (1)
Unit cell parameters:				
<i>a</i> , Å	16.7805(7)	4.366(4)	12.7857(3)	5.2092 (7)
<i>b</i> , Å	4.9693(2)	36.870(4)	10.0036(5)	6.5158 (7)
<i>c</i> , Å	8.9798(4)	5.0970(15)	14.1379(6)	16.599 (3)
α , deg	90	90	90	99.154(11)
β , deg	90.898(4)	98.49(6)	90	93.532(11)
γ , deg	90	90	90	98.482(10)
<i>V</i> , Å ³	748.71(5)	811.5(8)	1808.28(13)	548.06 (13)
<i>Z</i>	2	2	4	1
<i>D</i> _x , g cm ^{−3}	1.367	1.377	1.338	1.274

^a Determined by DSC.

1–4 and their corresponding 2D fingerprint plots are shown in Fig. 5. The relative contributions of each interaction to the Hirshfeld surface are depicted in Fig. 6. d_{norm} mapped on Hirshfeld surface for visualizing the intermolecular interactions between the molecules of compounds **1–4** is presented in Figs. S1–S4. The detailed fingerprint plots produced to show the relative contribution of different intermolecular interactions to the Hirshfeld surface are shown in Fig. S5.

From Figs. 5 and 6 it results that the major contribution is from H···H (37–53.9%), O···H (29.3–42.9%) and C···H (10.6–16.9%). Other intercontacts N···H (0–1.8%), O···O (0.7–1.4%) and C···C (0–3.6%; 3.6% for **2**) contribute considerably less to the Hirshfeld surfaces. The proportion of H···H interactions has increased from **1** to **4** since the longer amino acid chain affords a higher proportion of hydrogen atoms in the structure. Thus, compound **1** shows the lowest proportion of H···H interactions (37%) and the highest O···H contacts (42.9%). Conversely, the terephthalamide **4** contains the smallest proportion of O···H contacts (29.3%) and the highest proportion of H···H contacts (53.9%) reflected in the lowest crystal density (1.274 g cm^{−3}) compared to the other compounds. The sharp spike appearing in the middle of scattered points in the fingerprint map of **1** ($d_e = d_i = \sim 1.1$ Å) is from H···H interactions of the hydrogen from methyl ester moieties (H1A···H1A 2.281 Å). Of the compounds **1–4**, compound **2** contains the lowest contribution of C···H contacts (10.6%) due to the considerable distances between

Table 2
Hydrogen-bond geometry in terephthalamides **1–4**.

	D–H···A	D–H (Å)	H···A (Å)	D···A (Å)	D–H···A (°)
1	N1–H1···O3 ^a	0.86	2.08	2.8688(16)	152.9
	C3–H3A···O2 ^b	0.97	2.42	3.327(2)	155.5
2	N1–H1···O3 ^c	0.86	2.14	2.955(3)	157.4
	C3–H3A···O3 ^c	0.97	2.52	3.249(3)	131.7
3	N1–H1···O3 ^d	0.86	2.08	2.8650(16)	151.6
	C3–H3B···O2 ^e	0.97	2.74	3.448(2)	130.5
4	N1–H1···O3 ^f	0.86	2.22	3.0608(16)	164.7
	C3–H3A···O2 ^g	0.97	2.57	3.511(3)	164.6

Symmetry code(s).

^a $x, -1 + y, z$.

^b $x, 1/2 - y, 1/2 + z$.

^c $x, y, -1 + z$.

^d $1/2 - x, -1/2 + y, z$.

^e $1 - x, -1/2 + y, 1/2 - z$.

^f $-1 + x, y, z$.

^g $1 + x, y, z$.

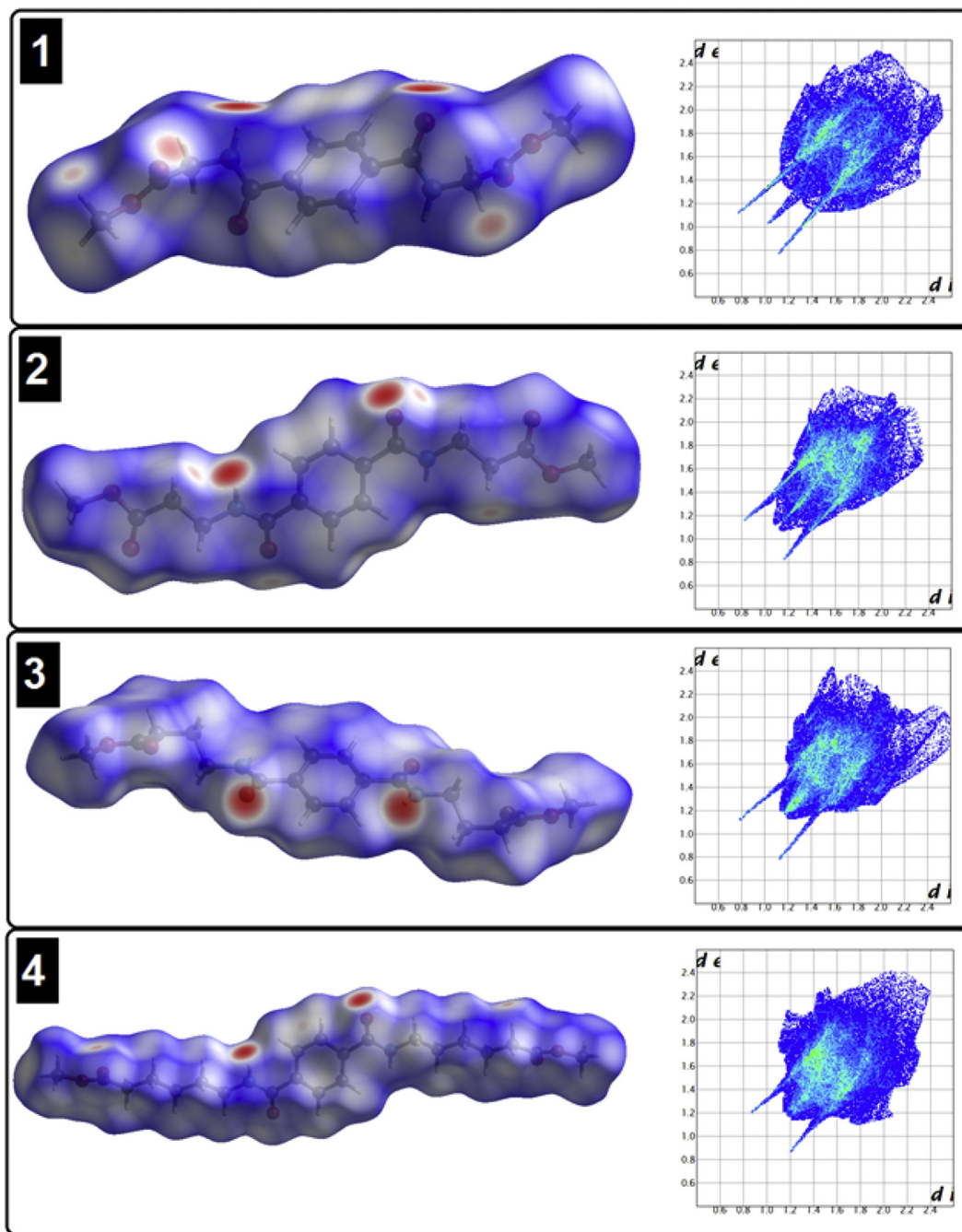


Fig. 5. (left) The Hirshfeld surfaces mapped with d_{norm} for the molecules of **1–4**. (right) The corresponding 2D fingerprint plots for the molecules of **1–4**.

neighboring molecules within one stack and between different stacks. Moreover, the length of b -axis is approximately eight times larger than those along the a -axis. In addition, compound **2** has the highest crystal density (1.377 g cm^{-3}).

A difference between the molecular interactions in compounds **1–4** in terms of $\text{O}\cdots\text{H}/\text{H}\cdots\text{O}$ interactions is reflected in the length of spikes (upper left and lower right at the bottom left of the plot). Thus, the spikes in the fingerprint of **4** reflect the shortest hydrogen bond ($\text{H}\cdots\text{O}$ 2.22 Å), while the length of spikes in the fingerprint of **1** and **3** is comparable ($\text{H}\cdots\text{O}$ 2.08 Å for **1** and **3**). These strong $\text{N}\cdots\text{H}\cdots\text{O}$ interactions between molecules of terephthalamides are visualized as bright red spots between the donor and acceptor atoms on the Hirshfeld surfaces in Figs. S1–S4. The characteristic

“wings” in the fingerprints are identified as a result of $\text{C}\cdots\text{H}$ contacts. The small contribution of a $\text{C}\cdots\text{H}$ interactions in the structure of **2** means that the wings are almost absent in its fingerprint 2D plot. The $\text{H}\cdots\text{H}$ contacts appear in the middle of scattered points in the fingerprint map of **1–4**.

2.3. Vibrational spectra of **1–4** terephthalamides with amino acids

ATR-FTIR spectra of pure compounds in the range of $4000\text{--}400 \text{ cm}^{-1}$ are shown in Fig. S6. The IR spectra of neat and deuterated solid-state samples **1–4** powdered in KBr pellets in the $\nu_{\text{N-H}}$ and $\nu_{\text{N-D}}$ band frequency ranges at two different temperatures are presented in Fig. 7. The IR spectra of the same samples recorded

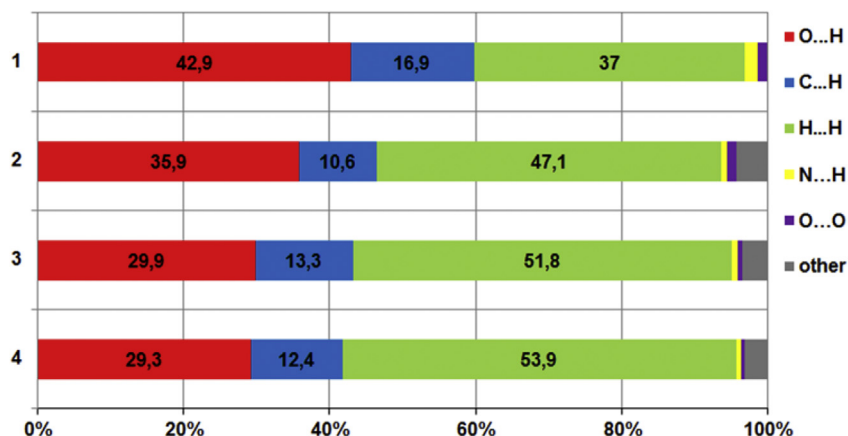


Fig. 6. The relative contributions of each interaction to the Hirshfeld surface in 1–4.

in the frequency range of 1800–1000 cm^{-1} are shown in Fig. S7. Comparing these IR spectra it can be observed that the procedure of sample preparation does not affect the IR spectra of terephthalamides. The Raman spectra, allowing to identify of the positions of the $\nu_{\text{C-H}}$ bands, are shown in Fig. S8.

The IR spectra of all compounds reveal the N–H amide stretching vibrations at around 3300 cm^{-1} (amide A) confirming the presence of amide sequences in the side chains. The relatively small difference between the positions of the $\nu_{\text{N-H}}$ stretching vibration band of associated amide groups indicates a similar strength of H-bonds in the crystals, which is confirmed in the structural data (Table 2). The lowest frequency of the $\nu_{\text{N-H}}$ band is observed for **1** (3292 cm^{-1}); the highest for **4** (3321 cm^{-1}). Hence, it is possible to conclude that H-bonds are stronger in the crystals of **1** than in **4**. For **3**, the frequency $\nu_{\text{N-H}}$ of the amide group at RT in IR

spectra recorded by different procedures is slightly higher than for **1**, although the corresponding N...O distance in the case of **3** is 0.04 Å smaller (Table 2). The very small band above 3400 cm^{-1} should be assigned to N–H out-of-phase stretching vibrations. The N–D amide stretching vibrations in IR spectra of deuterated compounds occur in the region 2550–2350 cm^{-1} .

Other characteristic bands for all compounds can be found at ~1730 cm^{-1} (ester carbonyl stretching vibrations), ~1633 cm^{-1} (amide carbonyl stretching vibrations; amide I), ~1540 cm^{-1} (in-plane N–H bending vibrations; amide II), 1396–1361 cm^{-1} (C–N amide stretching), peaks at 1205–1160 cm^{-1} (C–O stretching of esters) ~990 cm^{-1} (C–O torsion), 863–856 cm^{-1} (C–C stretching), 683–639 cm^{-1} (OCO bending) (Fig. S6–S7). The peaks at the lower region in the spectra at ~860 cm^{-1} suggest that the benzene ring is *para*-disubstituted. In the IR spectrum of **1**, the absorption bands of

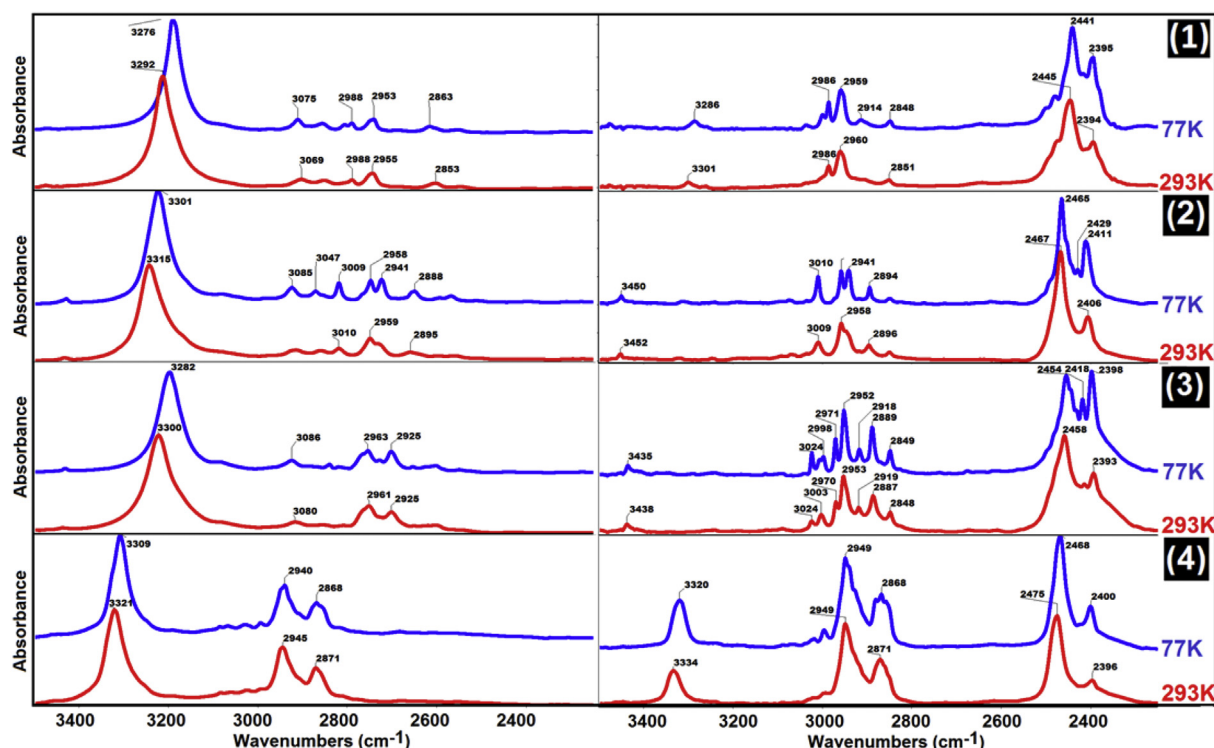


Fig. 7. IR spectra of (left) neat and (right) deuterated terephthalamides measured for a KBr pellets at (red) 293 and at (blue) 77 K in the 3500–2250 cm^{-1} frequency range.

C=O stretching vibrations of the ester group splits into two components at 1760 cm^{-1} and 1740 cm^{-1} , indicative of interactions by H bonding of the ester group (C1–H1B...O1 $3.724(3)\text{ \AA}$ and C1–H1C...O1 $3.725(4)\text{ \AA}$). According to the literature, the peaks in the region $3100\text{--}3000\text{ cm}^{-1}$ are assigned to C–H ring stretching vibrations. In our case, the peaks with very weak intensity are observed at 3069 and 3032 cm^{-1} (**1**), 3079 , 3040 and 3010 cm^{-1} (**2**) and 3080 cm^{-1} (**3**) attributed to C–H ring stretching vibrations in the IR spectra of a KBr pellet (Fig. 7). These peaks are not visible in ATR-IR spectra. The C–H in-plane ring bending vibrations appear in the region $1300\text{--}1000\text{ cm}^{-1}$ and the C–H out-of-plane bending vibrations in the range of $1000\text{--}750\text{ cm}^{-1}$ in the aromatic compounds.^{14–16} The ring aromatic carbon-carbon stretching vibrations occur in the region $1650\text{--}1400\text{ cm}^{-1}$ in benzene derivatives.^{14–16} For aromatic six membered rings, there are two or three bands in this region due to skeletal vibrations, the strongest usually being at about between 1500 and 1600 cm^{-1} .^{14–16} The frequencies of the asymmetric stretching for CH_2 and CH_3 are a magnitude higher than the frequencies of the symmetric stretching. Therefore, the asymmetric and symmetric stretching vibrations of CH_2 and CH_3 groups in the side chains have absorption bands at 2955 (**1**), 2959 (**2**), 2961 (**3**) 2945 cm^{-1} (**4**) and 2853 (**1**), 2895 (**2**), 2925 (**3**), 2871 cm^{-1} (**4**), respectively. With the growing length of the amino acid chain in the compounds, a gradual widening, increase in the relative intensity and shift of absorption bands corresponding to the vibrations of aliphatic C–H bonds is observed due to the formation of C–H...O hydrogen bonds. Interpretations of the IR spectra were based on previous works, found in the literature.^{17–21}

The characteristic Raman peaks for all terephthalamides were as follows: a weak band at $\sim 3300\text{ cm}^{-1}$ (stretching of the NH group), peaks with medium and very strong intensity above 3000 cm^{-1} (C–H ring stretching vibrations: 3073 and 3058 cm^{-1} for **1**; 3078 and 3038 cm^{-1} for **2**; 3073 cm^{-1} for **3** and 3074 and 3061 cm^{-1} for **4**), peaks in the range of $3000\text{--}2850\text{ cm}^{-1}$ (aliphatic C–H stretching: 2988 and 2952 for **1**; 2959 , 2943 , 2899 and 2851 cm^{-1} for **2**; 2961 , 2927 and 2874 cm^{-1} for **3**; 2951 , 2910 and 2874 cm^{-1} for **4**), a peak at $1734\text{--}1742\text{ cm}^{-1}$ (ester carbonyl stretching vibrations), a band at $1645\text{--}1633\text{ cm}^{-1}$ (amide carbonyl stretching vibrations), a peak at $\sim 1615\text{ cm}^{-1}$ (aromatic C–C stretching vibrations), a weak peak at $\sim 1570\text{ cm}^{-1}$ (N–H bending vibrations), $1345\text{--}1315\text{ cm}^{-1}$ (C–N amide stretching), $1163\text{--}1147\text{ cm}^{-1}$ (C–O ester stretching), below 1000 cm^{-1} (C–C skeleton vibrations, OCO and C–C–C bending vibrations) (Fig. S8). A comparison of compounds **1–4** shows the evolution of the band widths and shapes in the range of $3100\text{--}2800\text{ cm}^{-1}$ with the lengthening of side chain by a methylene groups. Hence, compound **4** has the highest proportion of aliphatic C–H relative to aromatic C–H in IR and Raman spectra. The assignment of Raman bands was based on previous works.^{19,22,23}

2.4. The temperature effects in IR spectra of the hydrogen bond

The temperature effect on the IR spectra of **1–4** as neat and deuterated solid-state samples powdered in KBr pellets in the $\nu_{\text{N-H}}$ and $\nu_{\text{N-D}}$ band frequency ranges is shown in Fig. 7. Fig. S9 shows the temperature dependent IR spectra of the most intense polarized components of the crystalline spectra in the ranges of the $\nu_{\text{N-H}}$ and the $\nu_{\text{N-D}}$ bands.

When the temperature changes from 293 K to 77 K , the IR spectra of terephthalamide samples exhibit a shift, an increase in the intensity and a decrease in the absorption band half-widths. After cooling, the absorption bands of the N–H stretching vibrations of the amide group shifted toward lower frequencies, indicating that the hydrogen bonds become shorter and more stable. For the IR spectra of the terephthalamide pellets with KBr, the effect

of a red shift of this band with cooling from 293 K to 77 K is much noticeable. The maximum shift is observed for **3** ($\Delta = 18\text{ cm}^{-1}$), the minimum shift takes place for **4** ($\Delta = 12\text{ cm}^{-1}$) ($\Delta = 16\text{ cm}^{-1}$ for **1**; $\Delta = 14\text{ cm}^{-1}$ for **2**) (Fig. 7). The frequencies of the stretching vibrations of the skeletal CH, side CH_2 and terminal CH_3 groups also change with temperature. The absorption bands of the C–H ring and C–H aliphatic stretching vibrations in compounds **1–3** are shifted to a higher frequency when the temperature is lowered from RT to 77 K . In the case of **4**, on cooling the crystals to 77 K , the positions of the maxima of aliphatic $\nu_{\text{C-H}}$ bands shift to the low-frequency region. Therefore, the C–H bonds in **4** probably become stronger on cooling. In view of our earlier results corresponding other amide systems (3-methyl- and 4-methylacetanilide,¹²ⁿ thioacetanilide and N-methylthiobenzamide²⁶), the terephthalamide crystal spectra exhibit similarly minor temperature effects in the region of $3500\text{--}2500\text{ cm}^{-1}$, i.e., the lower-frequency $\nu_{\text{N-H}}$ band branch remains less intense in the wide temperature range in comparison to the higher-frequency one. A decrease in temperature causes a decrease (by $\sim 4\text{ cm}^{-1}$) in the C=O ester and C=O amide stretching vibrations. At room temperature the absorption band of the N–H bending vibrations is observed in the IR spectrum at $\sim 1550\text{ cm}^{-1}$, while on cooling it shifts towards the high frequency region by 6 cm^{-1} . Other absorption bands in the IR spectra are also shifted by a smaller degree. Comparing the changes in the form and position of the $\nu_{\text{N-H}}$ absorption bands on cooling in the IR spectra of all compounds, one can conclude that the absorption bands of compounds are similarly sensitive to temperature variation as the side chain of compounds lengthens.

This is likely to be also explained by the presence of additional hydrogen bonding C–H...O engaging the carbonyl groups of terephthalamide which contribute towards the stability of the crystal packing.

Upon cooling, the higher-frequency branch of the N–D stretching vibrations of terephthalamides shifted toward lower frequencies, whereas the lower-frequency branch toward higher frequencies. In addition, the intensity of the shorter-wave branch of the $\nu_{\text{N-D}}$ band is higher than the longer-wave one for **1**, **2** and **4** at both temperatures. At 77 K , the $\nu_{\text{N-D}}$ stretching band of **3** changes the intensity ratio of its two spectral branches whose intensities are comparable (Fig. 7, Fig. S9).

The particular spectral behaviour of terephthalamides upon cooling results from the non-advantageous molecular electronic properties of terephthalamides, which prevent the effective activation of the “TH” mechanism even at low temperatures. Hence, the TS-type Davydov coupling involving pairs of closely-spaced hydrogen bonds in adjacent chains dominates at both temperatures. Only compound **3** does not confirm this regularity at whole.

In general, the magnitude of the TS-type exciton coupling involving the lateral spaced hydrogen bonds decreases when the number of the methylene groups associated to the terephthalamide system increases. Then the lower-frequency branch of the $\nu_{\text{N-H}}$ band reduces its intensity and the number of spectral bands from multiple peaks to two lines at 2940 and 2870 cm^{-1} . Additionally, the hydrogen bonding strength in terephthalamides also seems to influence the interplay of intra- and interchain exciton couplings. The N–H...O hydrogen bond between molecules in terephthalamide **3** is slightly stronger than in the other derivatives. As a result compound **3** exhibits an intrachain exciton coupling effect (TH-type), beyond the lateral exciton couplings of side-to-side-type, and the lower-frequency branch of the $\nu_{\text{N-D}}$ band appears with a noticeable high intensity. Compound **3** also displays a more complex temperature effect, depending on the intensity growth of the lower-frequency branch of the $\nu_{\text{N-D}}$ bands upon cooling. Conversely, the IR spectra of compound **4** (with the weakest

N–H...O hydrogen bond) shows a very weak lower-frequency branch of the $\nu_{\text{N-H}}$ and $\nu_{\text{N-D}}$ bands and also very weak temperature effects. Thus, only the TS-type coupling dominates in this particular case.

2.5. Infrared spectroscopy in polarized light of the hydrogen bond

The spectra of **1–4** single crystals in polarized light recorded in the $\nu_{\text{N-H}}$ and $\nu_{\text{N-D}}$ band frequency ranges for two polarizations of the electric field vector E , at 293 K and 77 K, are shown in Fig. 8.

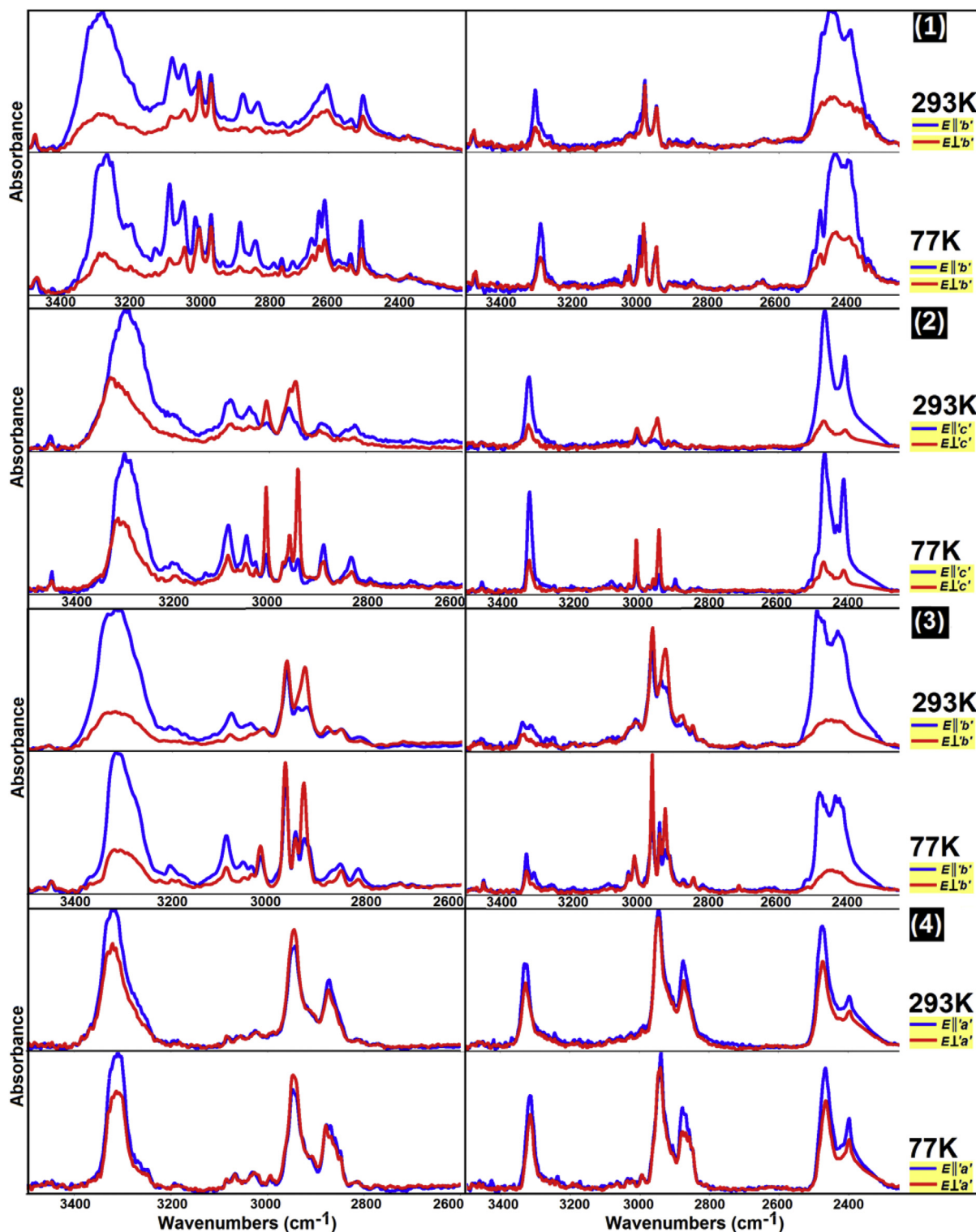


Fig. 8. Polarized IR spectra of (left) isotopically neat and (right) isotopically diluted crystals of **1–4** (1 10% H, 90% D; 2 10% H, 90% D; 3 10% H, 90% D; 4 40% H, 60% D), measured at 293 K and 77 K in the $\nu_{\text{N-H}}$ and $\nu_{\text{N-D}}$ band frequency ranges. (blue) The electric field vector E is parallel to the direction of hydrogen bond chains in the lattice ($E \parallel b'$ for 1 and 3, $E \parallel c'$ for 2, $E \parallel a'$ for 4); (red) $E \perp$ to the direction of hydrogen bond chains in the lattice.

All terephthalamides exhibit similar IR spectra, i.e., the distribution of absorption bands, frequencies and half-widths at maximum. The polarized IR spectra are characterized by fairly similar $\nu_{\text{N-H}}$ band contour shapes, i.e., the shorter-wave branch of the band ($3400\text{--}3150\text{ cm}^{-1}$) is of higher intensity than the intensity of the longer-wave spectral branch ($3150\text{--}2500\text{ cm}^{-1}$) (Fig. 8). Similarly, the higher-frequency branch of the $\nu_{\text{N-D}}$ band ($\sim 2460\text{ cm}^{-1}$) is of higher intensity than the intensity of the lower-frequency spectral branch ($\sim 2400\text{ cm}^{-1}$). Such intensity distribution in the absorption band is typical for the systems with non-aromatic hydrogen bonds.^{12l–12n} For each compound, differences can be observed between the spectra obtained with parallel and perpendicular polarization of light (the “first” kind of dichroic effect). When the IR polarization is parallel to the direction of hydrogen bond chains in the lattice ($E\parallel b$ for **1** and **3**, $E\parallel a$ for **2**, $E\parallel c$ for **4**), the peak of the $\nu_{\text{N-H}}$ stretching vibration at $\sim 3300\text{ cm}^{-1}$ is prominent, and an intensity of the shoulder in the region $3150\text{--}2500\text{ cm}^{-1}$, corresponding to the $\nu_{\text{C-H}}$ stretching vibrations, is considerably weaker. When the E vector polarization is perpendicular to the direction of hydrogen bond chains in the lattice ($E\perp b$ for **1** and **3**, $E\perp c$ for **2**, $E\perp a$ for **4**), the intensity of the longer-wave spectral branch ($3150\text{--}2500\text{ cm}^{-1}$) is higher or comparable to the intensity of the shorter-wave branch ($3400\text{--}3150\text{ cm}^{-1}$). Thus the dichroic properties of the band at $\sim 3300\text{ cm}^{-1}$ is different from that of the other absorption bands in this region, but similar to that of the amide I band at 1633 cm^{-1} . This clearly contains information about the relative orientations of the dipole moment changes associated with these vibrations. The observed intensity distribution of the IR bands depends upon the actual orientation of the oriented monocrystalline film with respect to the electric field vector of the polarized radiation.

Our earlier results have showed that in the polarized IR spectra of hydrogen bonds within the zig-zag chains, the intrachain vibrational exciton coupling leads to the characteristic linear dichroic effects, differentiating properties of the lower- and the higher-frequency branches of the $\nu_{\text{X-H}}$ bands (the second kind of dichroic effect).^{24,25} Thus, the individual band branch corresponds to the proton stretching vibrations in the chain exhibiting a different symmetry, i.e., the proton “in-phase” stretching vibration band is characterized by polarization of the transition moment vector parallel to the molecular chain direction; the excitation of the proton “out-of-phase” vibrations is polarized perpendicularly to the chain direction. Therefore a light non-proportionality of the intensity distribution in comparison to the component sub-bands of each polarized spectrum should be observed. In the case of our terephthalamides, the second kind of polarization effect is relatively weak in comparison to other systems with a chain arrangement of hydrogen bonds in their lattices even though amides molecules also form infinite, zig-zag-type open hydrogen bond chains. On the other hand, the IR spectra of the compounds significantly resemble the analogous spectra of other amides in the solid-state.^{12n,26}

2.6. H/D Isotope effect in the IR spectra of the hydrogen bond

The IR spectra of deuterated terephthalamides displayed a frequency shifts in the positions of some of the IR peaks in addition to changes in the relative intensities of the IR bands before deuteration (Fig. 9, Fig. S10).

FT-IR spectra of the terephthalamides upon deuteration reveal a number of spectral changes that include a marked change in the position of the C=O amide band between 1600 and 1700 cm^{-1} . A considerable decrease in the intensity of the N–H amide bending band, which is centered near 1550 cm^{-1} but it shifts down in

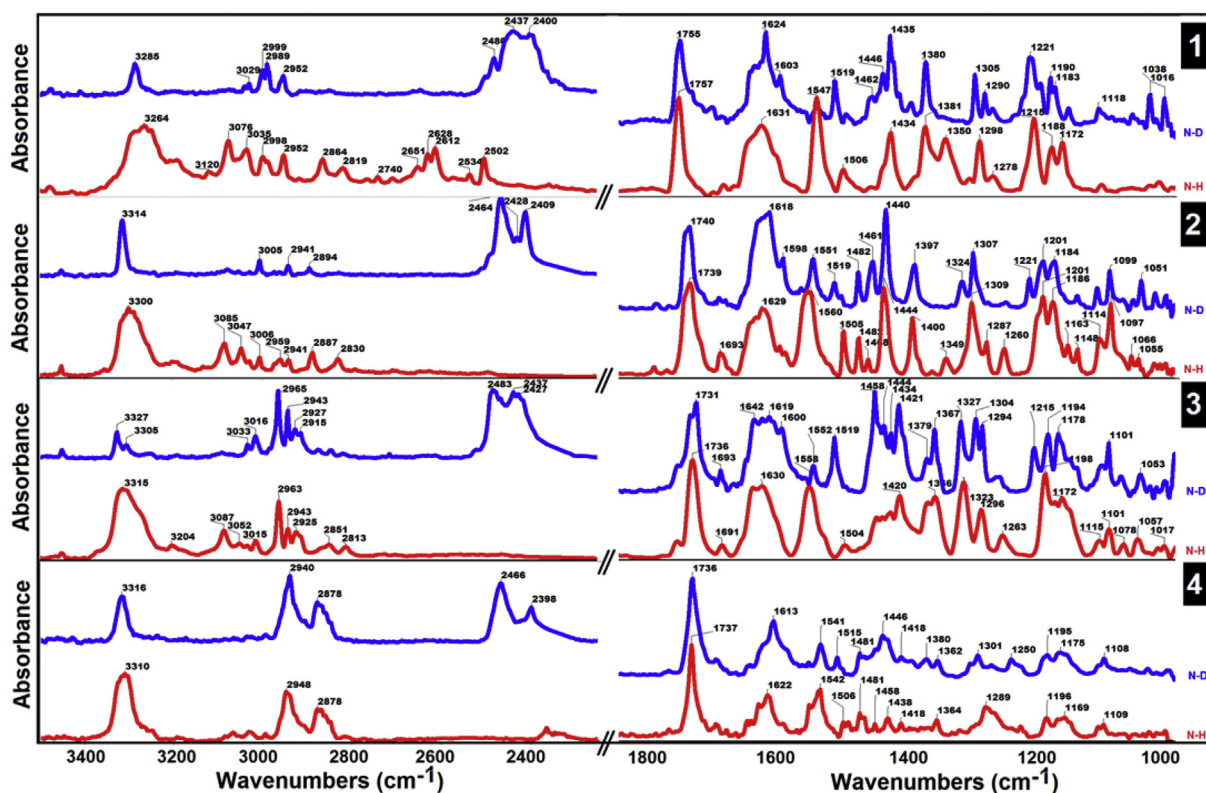


Fig. 9. Isotopic dilution effect in the polarized IR spectra of terephthalamides presented for the most intense polarized component bands at 77 K in the ranges of (left) $3500\text{--}2250\text{ cm}^{-1}$ and (right) $1850\text{--}1000\text{ cm}^{-1}$.

frequency upon deuteration to $\sim 1170\text{ cm}^{-1}$ was also observed. Replacement of a hydrogen atom by deuterium slightly weakens the H-bond strength (Ubbelohde effect).^{27,28} The $\nu_{\text{N-D}}$ absorption bands in the IR spectra are characterized by relatively simple fine structure patterns of frequencies related by the $1/\sqrt{2}$ factor with the corresponding frequency values of the spectral branches in the $\nu_{\text{N-H}}$ bands. This is the well-known H/D isotopic effect in the area of the IR spectroscopy of the hydrogen bond.

The absorption bands of N-D groups in the deuterated terephthalamides appear at $2477\text{--}2395\text{ cm}^{-1}$ and they also exhibit a two-branch structure, and qualitatively similar linear dichroic and temperature properties to those of the $\nu_{\text{N-H}}$ bands. The property of the $\nu_{\text{N-D}}$ absorption bands is almost proportional to the change in their intensity distribution when the polarization of the electric field vector “*E*” of the incident beam is changed in the experimental conditions. When the temperature is lowered from RT to 77 K, the absorption band of N-D stretching become sharp, well pronounced and red shifted. Moreover the higher-frequency branch of the $\nu_{\text{N-D}}$ bands is still more intense than the lower-frequency branch at both temperatures for compounds **1–3**.

A comparison of the IR spectra of the deuterated to the non-deuterated compounds in Fig. 9 shows the $\nu_{\text{N-H}}$ bands that are observed in both IR spectra. Most intriguing is the peak at $\sim 3300\text{ cm}^{-1}$, which gives unequivocal evidence for the presence of the “residual” protons, not replaced by deuterons during the isotopic exchange process. This peak is characterized by the invariability regardless of the growing isotopic exchange rates in the samples. Based on our publications, this phenomenon is associated with a non-random distribution of protons and deuterons in the lattice of hydrogen bonds of isotopically diluted crystals.¹¹ Then, all the vibrational exciton interactions involving the lateral spaced hydrogen bonds from the adjacent chains are retained in isotopically diluted crystals.

This spectacular isotope effect in terephthalamides has proved that the distribution of protons and deuterons depends on the interplay of intra-to interchain exciton couplings between hydrogen bonds in the crystalline lattice upon deuteration. Furthermore, the relative contribution of each individual exciton coupling mechanism in the spectra generation can be related to the strength of hydrogen bond. With increasing hydrogen bond strength the contribution of intrachain exciton coupling also increases (from **4**, **2**, **1** to **3**). Then, the two-branch structure of the $\nu_{\text{N-D}}$ band appears, the distribution of hydrogen isotopes between hydrogen bonds in deuterated **1–3** crystals is non-random and the dynamical co-operative interactions exist. Conversely, the distribution of protons and deuterons is random or partly random when only one very weak exciton coupling predominates in deuterated samples. Thus, the H/D isotopic “self-organization” effects in the spectra of **4** crystals are probably absent due to very weak TS-type exciton coupling involving hydrogen bonds in the deuterated crystal lattice.

3. Conclusion

We have synthesized and structurally evaluated new bis-terephthalamides **1–4** to obtain the non-conventional molecular systems whose spectral properties could deliver arguments for testing the contemporary models of the exciton interactions involving hydrogen bonds. The N–H \cdots O and C–H \cdots O hydrogen bond interactions were found in four individual molecular systems. It is evident from our spectral results that the $\nu_{\text{N-H}}$ band of terephthalamides is sensitive to the substituent, the temperature and the isotopic dilution. The two-branch structure of the $\nu_{\text{N-H}}$ and $\nu_{\text{N-D}}$ bands with their unique intensity distribution patterns, the polarization and temperature effects observed in the IR

spectra of terephthalamide crystals indicate that the strongest exciton couplings are via the van-der-Waals forces as “through-space” ((TS)-coupling) engaging the laterally spaced hydrogen bonds from neighbouring molecular chains. With the lengthening of the side chain by methylene groups in **1–4** derivatives, the interchain TS-type coupling involving the closely-spaced hydrogen bonds, weakens. After cooling, the hydrogen bonds become strengthened and the $\nu_{\text{N-H}}$ and $\nu_{\text{N-D}}$ bands are shifted toward lower frequencies. Moreover, the intensity of the lower-frequency branch of the $\nu_{\text{N-D}}$ bands increases with the growth of the hydrogen bond strength upon cooling. This fact is connected with the growth of relative contribution of intrachain TH-type exciton coupling in the spectra generation in deuterated amide samples at 77 K. The deuteration process of the amide groups is evidenced by a growth in the intensity of the $\nu_{\text{N-D}}$ band two-branch structure pattern. The strength and the mutual ratio of intra-to interchain exciton couplings have a significant impact on the occurrence of the H/D isotopic “self-organization” phenomenon. In compounds **1–3** identical H isotope atoms, protons or deuterons, occupy the independent pairs of opposite, closely-spaced H-bonds, each belonging to a different chain in the crystals because the exciton couplings are strong enough. For compound **4** the TS-type exciton coupling is very weak and then the longer-wave branch of $\nu_{\text{N-D}}$ band nearly disappears. This is probably due to a fragmented disorder in the arrangement of proton and deuterons in the lattice of hydrogen bonds of **4**. In this case the H/D isotopic “self-organization” effects in the spectra of crystals of **4** are absent.

4. Experimental section

4.1. Materials and reagents

All reagents (Fluka, Merck) were of analytical grade and used without any further purification.

4.2. Synthesis of bis-terephthalamides

Terephthalamides **1–4** were synthesized by using the general procedure: the relevant amino acid methyl ester hydrochloride (22 mmol) was suspended in CH_2Cl_2 or CH_3Cl (100 ml) under argon atmosphere at 0°C . The mixture stirred for 30 min. Triethylamine (6 ml) was carefully added to the mixture, and stirred for 30 min. Terephthaloyl chloride (11.7 mmol) in CH_2Cl_2 or CH_3Cl (30 ml) was slowly added to the mixture, and then stirred for 2 h at room temperature. The reaction mixture was washed three times with H_2O . The organic residues were dried over anhydrous sodium sulfate, filtered and evaporated to give a solid. The crude product was recrystallized from CH_2Cl_2 . The final compounds were characterized by IR and Raman spectroscopy, ^1H NMR and ^{13}C NMR spectroscopy and mass spectrometry. Evaporation of a D_2O solution of each compound at room temperature and under reduced pressure allowed us to obtain its deuterium-bonded derivative. It appeared that the deuterium substitution rates for the $\nu_{\text{N-H}}$ groups for the title systems varied in the following ranges: 90–99% D and 10–1% H for **1–3** and 60% D and 40% H for **4**.

Terephthalamide **1**. White powder, Yield (1.893 g, 65%), mp 165°C ; ^1H NMR (400 MHz, CDCl_3) δ : 7.85 (s, 4H), 6.82 (br s, 2H), 4.25 (d, $J = 5.1\text{ Hz}$, 4H), 3.81 (s, 6H); ^{13}C NMR (101 MHz, CDCl_3) δ : 170.4, 166.5, 136.6, 127.4, 52.5, 41.8; IR (KBr): $\nu = 3288$ (s), 2988(w), 2954(w), 2852(w), 1740(s), 1633(s), 1539(s), 1502(w), 1434(w), 1422(w), 1374(m), 1329(w), 1296(w), 1272(w), 1025(m), 1183(m), 1167(m), 1073(w), 998(w), 872(w), 863(w), 745(w), 665(m), 532(w), 515(w) cm^{-1} ; MS (ESI) m/z calculated for $\text{C}_{14}\text{H}_{16}\text{N}_2\text{O}_6$: 309.29, found m/z : 309.52 [MH^+].

Terephthalamide **2**. White powder, Yield (1.674 g, 52%), mp 217 °C; ¹H NMR (400 MHz, CDCl₃) δ: 7.81 (s, 4H), 6.91 (br s, 2H), 3.76–3.72 (m, 4H), 3.72 (s, 6H), 2.67 (t, *J* = 5.9 Hz, 4H); ¹³C NMR (101 MHz, CDCl₃) δ: 173.4, 166.4, 137.0, 127.3, 51.9, 35.4, 33.6; IR (KBr): ν = 3312(s), 3012(w), 2959(w), 2895(w), 1735(s), 1632(s), 1547(s), 1502(m), 1433(s), 1341(m), 1305(m), 1196(m), 1177(m), 1159(m), 1092(w), 998(w), 891(w), 856(m), 732(w), 646(w), 425(w) cm⁻¹; MS (ESI) calculated for C₁₆H₂₀N₂O₆ *m/z*: 337.35, found *m/z*: 337.63 [MH⁺].

Terephthalamide **3**. White powder, Yield (2.915 g, 84%), mp 184 °C; ¹H NMR (400 MHz, CDCl₃) δ: 7.83 (s, 4H), 6.72 (br s, 2H), 3.67 (s, 6H), 3.55–3.50 (m, 4H), 2.47 (t, *J* = 6.9 Hz, 4H), 2.01–1.95 (m, 4H); ¹³C NMR (101 MHz, CDCl₃) δ: 174.3, 166.7, 137.0, 127.2, 51.9, 39.9, 31.8, 24.3; IR (KBr): ν = 3296(s), 2960(w), 2926(w), 1729(s), 1629(s), 1544(s), 1439(m), 1375(w), 1319(s), 1287(m), 1267(m), 1253(m), 1196(m), 1162(m), 933(w), 883(w), 860(w), 683(w) cm⁻¹; MS (ESI) calculated for C₁₈H₂₄N₂O₆ *m/z*: [MH⁺] 365.40, found *m/z*: 365.72.

Terephthalamide **4**. White powder, Yield (3.085 g, 77%), mp 147 °C; ¹H NMR (400 MHz, DMSO-*d*₆) δ: 8.55 (t, *J* = 5.6 Hz, 2H), 7.89 (s, 4H), 3.57 (s, 6H), 3.27–3.23 (m, 4H), 2.31 (t, *J* = 7.4 Hz, 4H), 1.59–1.50 (m, 8H), 1.34–1.29 (m, 4H); ¹³C NMR (101 MHz, DMSO-*d*₆) δ: 173.8, 165.9, 137.2, 127.5, 51.6, 39.5, 33.7, 29.2, 26.4, 24.6; IR (KBr): ν = 3316(s), 2943(mw), 2870(w), 1733(s), 1623(s), 1537(s), 1497(w), 1436(w), 1361(w), 1278(w), 1235(w), 1165(m), 1106(w), 861(w), 732(w), 639(w) cm⁻¹; MS (ESI) calculated for C₂₂H₃₂N₂O₆ *m/z*: 421.51, found *m/z*: 421.94 [MH⁺].

4.3. Characterization

The FT-IR spectra using ATR technique were recorded on a Nicolet™ iS™ 50 FT-IR (Thermo Scientific) spectrometer with a diamond attenuated total reflectance (ATR) module. One hundred scans were collected for each measurement over the spectral range of 4000–400 cm⁻¹ with a resolution of 4 cm⁻¹. Absorptions are denoted as follows: strong (s), medium (m), and weak (w) in the synthesis section. FT-IR spectra (4000–400 cm⁻¹) using the KBr pressed disk technique were conducted using a FT-IR Nicolet Magna 560 spectrometer with a resolution of 4 cm⁻¹ at two temperatures (293 K and 77 K). For each sample, 3 mg terephthalamide and 150 mg dried KBr were weighted and then were ground in an agate mortar. Polarized IR spectra (4000–400 cm⁻¹) were also recorded on a FT-IR Nicolet Magna 560 spectrometer between 4000 and 400 cm⁻¹ (200 scan, resolution 4 cm⁻¹) with the use of an IR polarizer (The Spectra-Tech IR Polarizer). The spectra of isotopically pure and deuterated compounds, in KBr pellet and as monocrystalline samples, at low temperature were taken using a standard cryostat system. For the aim of the experimental study, melts of very small quantities of the sample between CaF₂ windows were cooled by applying a suitable temperature gradient to obtain oriented films. Monocrystalline fragments were selected from the crystalline films and spatially oriented, using a polarization microscope (Nikon Eclipse E200). Samples were then exposed for the experiment by placing them on a metal plate diaphragm with a 1.5 mm diameter hole. Measurements of the polarized spectra of the compounds were performed for two different orientations of the electric field vector “*E*” with respect to an individual crystal lattice (the polarization angle 0 and 90) and were repeated for ca. ten different single crystals of a given compound. Raman measurements were made using a Thermo Scientific™ DXR™2xi Raman imaging microscope. The data were collected using a 532 nm laser and the power on samples was a 10 mW. A Raman microscope (Olympus BX-KMA-LED), equipped with a 50 × objective, was used for these wavelengths. ¹H and ¹³C NMR spectra were recorded on a Bruker Avance 400 MHz spectrometer.

Mass spectra were carried out on an Agilent (Varian) 500-MS IT Mass Spectrometer. Melting points were determined on a Bötius PHMK (VEB Analytik Dresden) apparatus.

4.4. X-ray crystallography

Single crystals used for X-ray measurements were obtained from acetone (**1**) and methanol (**2**, **3**) by slow evaporation of solvent at room temperature. Slow crystallization from CHCl₃–ethanol solution over a period of several days at 5 °C (refrigerated) afforded single crystals of **4**.

The data were collected using an Oxford Diffraction kappa diffractometer with a Sapphire3 CCD detector and SuperNova kappa diffractometer with an Atlas CCD detector. The crystals were mounted on a quartz glass capillary and measured at 298 K. Accurate cell parameters were determined and refined using the program CrysAlis CCD.^{29,30} For the integration of the collected data the program CrysAlis RED was used.^{29,30} Structures were solved using direct methods with the SHELXS-2013 program and then the solutions were refined with the SHELXL-2014/6 program.³¹ Non-hydrogen atoms were refined with anisotropic displacement factors. Hydrogen atoms were treated as “riding” on their parent carbon atoms with *d*(C–H) = 0.96 Å and *U*_{eq} = 1.5 *U*_{eq}(C) for methyl groups or with *d*(C–H) = 0.97 Å and *U*_{eq} = 1.2 *U*_{eq}(C) for methylene groups or with *d*(C–H) = 0.93 Å and *U*_{eq} = 1.2 *U*_{eq}(C) for aromatic H and N–H atoms. The details relating to the atomic coordinates, complete geometry of molecules and all crystallographic data are deposited at the Cambridge Crystallographic Data Center (CCDC No. 1005546–1005548 (**1–3**) and 1511353 (**4**)).³²

4.5. Hirshfeld surface analysis

The close contacts in the crystals of terephthalamides **1–4** were quantified using computational Hirshfeld surface analysis and their associated 2D fingerprint plots with the help of the CrystalExplorer 3.1 software on the basis of crystal structures.³³ Molecular Hirshfeld surfaces in the crystal structures were constructed on the basis of the electron distribution calculated as the sum of spherical atom electron densities.^{34,35} The graphical plots of the molecular Hirshfeld surfaces mapped with *d*_{norm} used a red-white-blue colour scheme, where white regions represented molecular contacts around the van der Waals distance, red highlighted shorter contacts, and blue was for contacts longer than the van der Waals distance.

Appendix A. Supplementary data

Supplementary data related to this article can be found at <http://dx.doi.org/10.1016/j.tet.2017.03.080>.

References

- Rodríguez-Galán A, Franco L, Puiggali J. In: Felton GP, ed. *Biodegradable Polymers: Processing, Degradation and Applications*. New York: Nova Press; 2011: 207–272. Ch. 4.
- Rodríguez-Galán A, Franco L, Puiggali J. *Polymers*. 2011;3:65.
- Fonseca AC, Gil MH, Simões PN. *Prog Polym Sci*. 2014;39:1291.
- Karimi P, Rizkalla AS, Mequanint K. *Materials*. 2010;3:2346.
- Sava I. *Polimery*. 2011;56:261.
- (a) Jones PG, Kuś P. *Z Naturforsch B*. 2011;66b:397; (b) Jones PG, Kuś P. *Z Naturforsch B*. 2011;66b:83; (c) Jones PG, Ossowski J, Kuś P. *Z Naturforsch B*. 2002;57b:914; (d) Kuś P, Borek J, Jones PG. *Acta Cryst C*. 2010;66:o93; (e) Ossowski J, Kuś P, Näther C, Jones PG. *Acta Cryst C*. 2006;62:o369.
- Ray S, Hegde RP, Das AK, Shamala N, Banerjee A. *Tetrahedron*. 2006;62:9603.
- Armelin E, Escudero E, Campos L, Puiggali J. *Acta Cryst C*. 2001;57:172.
- Majerz I, Gutmann M. *RSC Adv*. 2015;5:95576.
- Flakus HT, Bańczyk A. *J Mol Struct*. 1999;476:57.
- Flakus HT. *J Mol Struct*. 2003;646:15.

12. (a) Flakus HT, Hachuta B, Garbacz A. *J Phys Chem A*. 2012;116:11553;
(b) Flakus HT, Hachuta B, Majchrowska A. *J Phys Chem A*. 2012;116:7848;
(c) Rezik N, Ghalla H, Flakus HT, Jabłońska M, Blaise P, Oujia B. *ChemPhysChem*. 2009;10:3021;
(d) Najeh R, Houcine G, Flakus HT, Jabłońska M, Brahim O. *J Comput Chem*. 2010;31:463;
(e) Flakus HT, Rezik N, Jarczyk A. *J Phys Chem A*. 2012;116:2117;
(f) Rezik N, Flakus HT, Jarczyk-Jędryka A, et al. *J Phys Chem Solids*. 2015;77:68;
(g) Hachuta B, Flakus HT, Polasz A. *Spectrochim Acta A*. 2014;120:287;
(h) Hachuta B, Flakus HT, Polasz A. *Spectrochim Acta A*. 2014;126:333;
(i) Hachuta B, Jabłońska-Czapla M, Flakus HT, Nowak M, Kusz J. *Spectrochim Acta A*. 2015;134:592;
(j) Hachuta B, Flakus HT, Garbacz A, Stolarczyk A. *Spectrochim Acta A*. 2014;123:151;
(k) Flakus HT, Hachuta B, Stolarczyk A. *Spectrochim Acta A*. 2012;85:7;
(l) Flakus HT, Hachuta B, Pyzik A. *Chem Phys*. 2011;379:73;
(m) Flakus HT, Hachuta B. *Chem Phys*. 2010;368:133;
(n) Flakus HT, Śmiszek-Lindert W, Hachuta B, Michta A. *Spectrochim Acta A*. 2012;97:263.
13. Etter MC, MacDonald JC, Bernstein J. *Acta Cryst B*. 1990;46:256.
14. Karthikeyan N, Joseph Prince J, Ramalingam S, Periandy S. *Spectrochim Acta A*. 2015;139:229.
15. Karabacak M, Cinar M, Unal Z, Kurt M. *J Mol Struct*. 2010;982:22.
16. Téllez CA, Hollauer E, Mondragon MA, Castano VM. *Spectrochim Acta A*. 2001;57:993.
17. Kumar S, Rai AK, Singh VB, Rai SB. *Spectrochim Acta A*. 2005;61:2741.
18. Gómez-Zavaglia A, Fausto R. *Phys Chem Chem Phys*. 2003;5:3154.
19. Baran J, Ratajczak H. *Spectrochim Acta A*. 2005;61:1611.
20. Jun Yu S, Hyun Baik D, Gyu Jeong Y. *Fibers Polym*. 2014;15:2447.
21. Chen X, Cai X. *J Therm Anal Calorim*. 2016;125:313.
22. Zhu G, Zhu X, Fan Q, Wan X. *Spectrochim Acta A*. 2011;78:1187.
23. Jenkins AL, Larsen RA, Williams TB. *Spectrochim Acta A*. 2005;61:1585.
24. Flakus HT, Machelska A. *Spectrochim Acta A*. 2002;58:553.
25. Flakus HT, Tyl A, Jones PG. *Spectrochim Acta A*. 2002;58:299.
26. Flakus HT, Hachuta B, Turek E, Michta A, Śmiszek-Lindert W, Lodowski P. *Chem Phys Lett*. 2015;634:113.
27. Ubbelohde AR, Gallagher KJ. *Acta Cryst*. 1955;8:71.
28. Jeffrey GA. *An Introduction to Hydrogen Bonding*. New York: Oxford University Press; 1997.
29. CrysAlis CCD, CrysAlis RED. Version 1.171.29. Wrocław: Oxford Diffraction Ltd; 2008.
30. CrysAlisPRO. Version 1.171.36.28. Yarnton: Agilent Technologies; 2011.
31. Sheldrick GM. *Acta Cryst C*. 2015;71:3.
32. CCDC-1005546-1005548 (1-3) and 1511353(4) contain the crystallographic data for the structural analysis of terephthalamides. These data can be obtained from the Cambridge Crystallographic Data Centre (CCDC), 12 Union Road, Cambridge CB2 1EZ, UK (Fax: +44-1223-336033, www: <http://www.ccdc.cam.ac.uk>).
33. Wolff SK, Grimwood DJ, McKinnon JJ, et al. *CrystalExplorer 3.1*. University of Western Australia; 2012.
34. Spackman MA, Byrom PG. *Chem Phys Lett*. 1997;267:215.
35. Spackman MA, Jayatilaka D. *CrystEngComm*. 2009;11:19.